J. Fluid Mech. (1974), *vol.* 62, *part* 1, *pp.* 41–64
Printed in Great Britain

Physical characteristics of subsonic jets in a cross-stream

By P. CHASSAING, J. GEORGE, A. CLARIA AND F. SANANES

L'Institut de Mécanique des Fluides, 2 rue Charles Camichel, Toulouse, France

(Received 23 April 1973)

This paper deals with local flow characteristics of subsonic turbulent jets in the presence of a cross-flow. For the various types of jet considered (a cylindrical jet and coaxial jets) the experimental results concern the axes and the velocity profiles in the plane of symmetry of the flow. In the case of the cylindrical jet, the shape of the universal axial velocity profile is defined, as are the law of velocity decay along the axis and the laws of variation of the thicknesses of the jet. Finally, the existence of a link between the axis equation and the law of axial velocity decay in the zone of similarity of the velocity profiles is established.

1. Introduction to the problem

The prime motivation for understanding the mixing which takes place when a jet of fluid is affected by the shear of a cross-flow is its direct application to the problem of the emission of effluents into the atmosphere via a chimney. Observation of the behaviour of a wreath of smoke shows that rapid diffusion occurs in a natural wind, and it is obvious that this efficient entrainment mechanism should be thoroughly understood to enable it to be adapted to other systems; in other words the aim is to discover the coupling characteristics of turbulence of various intensities and scales.

In considering the problem of a jet in a cross-flow Ruggeri and Callaghan, in a series of publications (Callaghan & Ruggeri 1948, 1951; Ruggeri, Callaghan & Bowden 1950; Ruggeri 1952), studied the effect of varying the shape of the orifice and of heating the jet on a two-dimensional flow. Jordinson (1956) was the first to determine experimentally the trajectory of the wreath, defined the axis as the line joining the points of maximum velocity, and demonstrated that the cross-section of an initially cylindrical jet is distorted by the shear flow into a horseshoe shape. Gordier (1959), working with water, showed that Reynolds similarity could be applied. Keffer & Baines (1963) studied the structure of the turbulence in a deflected jet and showed that similarity for the mean velocity profiles could be defined. Fan (1967) introduced the effect of a stratified atmosphere and suggested a mathematical model based on the resistance caused by the smoke wreath in the flow. Platten & Keffer (1968) suggested a model taking into consideration the two entrainment effects occurring in a deflected jet.

In this paper, the object is to extend the problem to the case of multiple jets,

in order to understand more fully the turbulent mixing phenomena. It begins by considering the overall effects, which are easier to appreciate; but the essential characteristics of turbulent coupling must be considered to allow a better understanding of this complex phenomenon.

2. Study of a single jet

The major drawback of past theories, including those of the Russian school, represented in particular by Abramovitch (1963), Shandorov (1966) and Akatnov (1969), results from the overall level chosen for analysing the phenomenon, which does not take into account the finer characteristics, such as the axial velocity profile for example.

Now, in the plane of symmetry, at least, it is possible to separate experimentally a certain number of properties of the characteristics of the flow, amongst which figures the similarity of the profiles in question.

The problem which presents itself is then that of the compatibility of the solution obtained for the axis of the jet from overall hypotheses with the real properties of the flow. In order to discuss this in more detail, it is necessary to give the picture of the flow in the plane of symmetry as obtained from the experimental results.

2.1. *The behaviour of the jet in the presence of a cross-flow*

As in the case of a jet flowing into a calm atmosphere, three distinct zones can be distinguished in the evolution of the jet in the presence of a cross-flow (see figure 1).

Right from the outlet section, at which the vertical velocity profile is relatively uniform and the turbulent intensity is low, the jet undergoes strong shearing constraints owing to the velocity gradient. However, unlike the case of a jet without cross-flow, the velocity gradient cannot be reduced to a single resultant, so that the entrainment, which in the first case was uniform and axisymmetric, now reveals itself to be far more complex.

Moreover, as long as the jet possesses a relatively high amount of energy, it constitutes, for the external flow, a real obstacle, so that the overall flow which is established is the result of two flows: that of the external fluid around an obstacle characterized in particular by a region of eddies in the wake and that of the initially cylindrical jet normal to the direction of the external flow at infinity.

The presence of this wake zone, in which a whirling system of low frequency relative to that of the turbulent disturbance is generally established, is the main cause of the asymmetry of the jet, resulting from the asymmetry of the intermittent zone surrounding the boundary of the latter, and of the asymmetry of the rate of entrainment into the external fluid.

Thus, in zone I, called the *zone of residual inlet velocity*, the external fluid starts to be entrained by the jet, which in consequence spreads, slows down and curves. The characteristic of this zone is that only the circumferential part of the jet takes part in the mixing, the remainder forming the potential core,

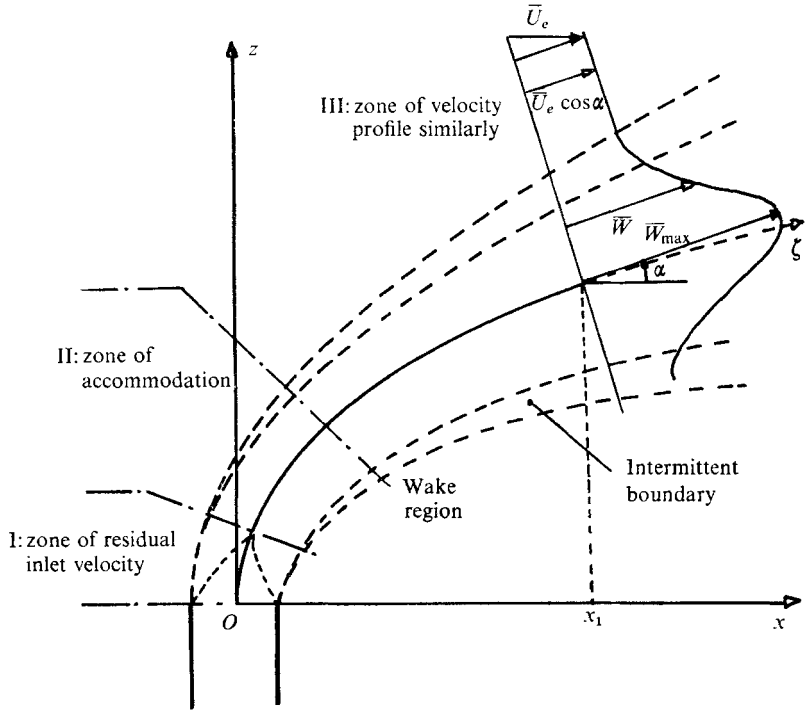

FIGURE 1. Configuration of the flow in the plane of symmetry.

where the axial velocity is of constant magnitude, but because of the initiation of the curve, this core no longer forms a cone strictly speaking, as was the case in a calm atmosphere. In practice, however, it was observed for the range of speeds considered that this zone is much less extensive than for the jet in a calm atmosphere, and thus that the curvature is sufficiently small for this potential core to be approximated by a cone without introducing significant error.

When the maximum axial velocity begins to decrease, zone II, known as the *zone of accommodation*, is reached; this zone is characterized by, amongst others, the following properties: the curvature of the jet increases; the entire section participates in the turbulent mixing.

Zone III, that of *velocity profile similarity*, appears when a law of similarity can be established for the velocity profiles. It will be discussed in greater detail in §§2.4 and 2.6.

2.2. *Raw exploratory results*

In all the tests, the velocity profile $\overline{U}_e$ was uniform at infinity and the level of turbulence of the transverse flow was less than 1 %. The jet was obtained by using a cylindrical tube of radius $r_0 = 2$ cm and length $120r_0$ supplied by filtered air. The velocity profile in the outlet plane then corresponded closely with that of fully developed turbulent flow in a smooth pipe, the initial Reynolds number Re_0 based on the diameter lying between 21 200 and 53 600, depending on the test.

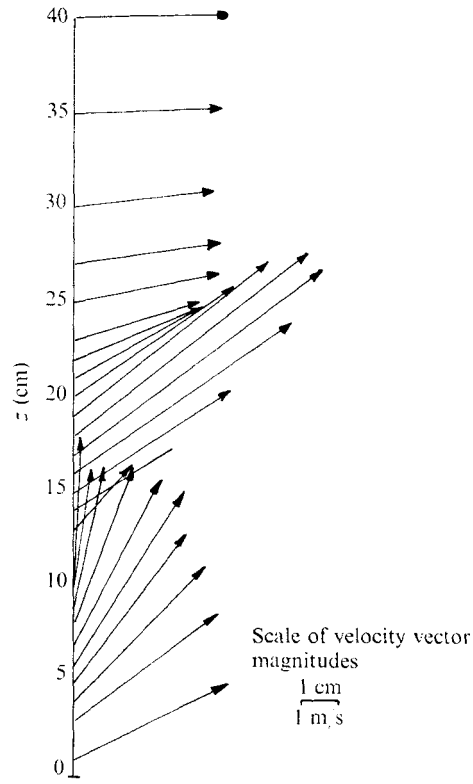

FIGURE 2. Raw results of the exploration of a cylindrical jet deflected by a cross-flow. Example of velocity field measurement. Test characteristics: $\overline{W}_{m0} = 16{\cdot}95\,\mathrm{m/s}$; $a = 3{\cdot}95$; $Re_0 = 41\,500$.

Using simultaneous measurement techniques the direction of the flow was measured using pressure sensors, and hot-wire anemometry was used for the magnitude of the flow to obtain the velocity profiles at various sections $x = x_i$ of the plane of symmetry of the flow. In each case a vector diagram similar to that of figure 2 was obtained.

2.3. *Axis of the jet*

For each section $x = x_i$, the co-ordinate z of the point where the magnitude of the velocity vector is a maximum can be determined from the preceding result. The locus of these points in the plane of symmetry of the flow is, by definition, the axis of the jet.

Figure 3 gives the experimental curves obtained for three different values of the ratio $a = \overline{W}_{m0}/\overline{U}_e$ of the mean exit velocity over the velocity of the cross-flow equal to 2·37, 3·95 and 6·35 respectively. As shown by figure 4 these axes coincide at a certain distance from the origin with a curve given by the equation

$$z/r_0 = A(x/r_0)^{0{\cdot}385}, \tag{1}$$

where

$$A = 1{\cdot}53 + 0{\cdot}90(\overline{W}_{m0}/\overline{U}_e). \tag{2}$$

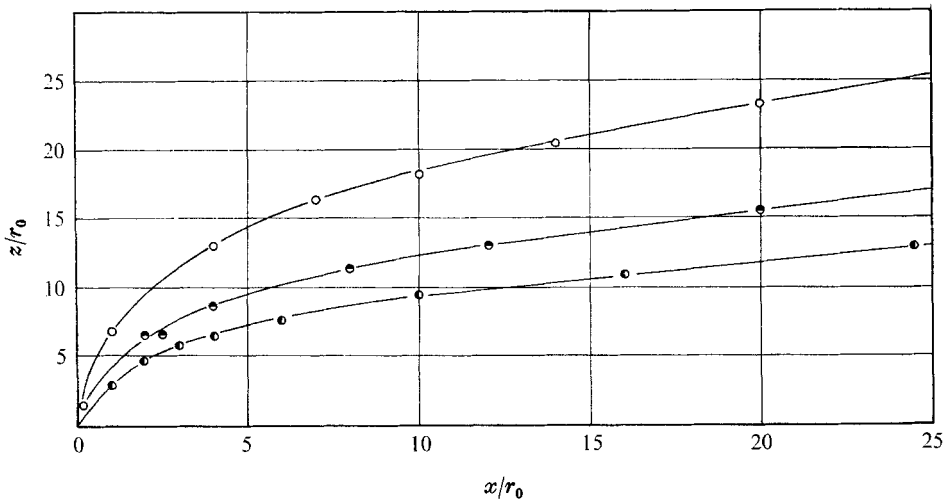

FIGURE 3. Jet axis ○, $a = 6{\cdot}35$; ◓, $a = 3{\cdot}95$; ◐, $a = 2{\cdot}37$.

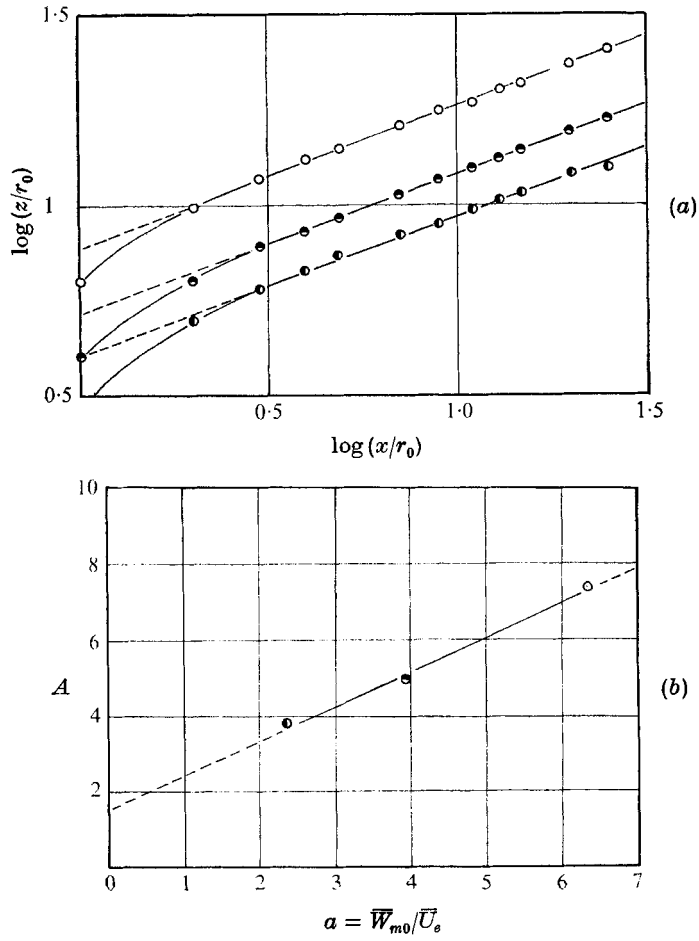

FIGURE 4. Calculation of jet axis. Slope of linear part in (*a*) is 0·385.
$z/r_0 = A(a) \times (x/r_0)^n$.

	Value of n	Values of α and β; $A = Ka^{\alpha}+\beta$	Notes on sources of results
Keffer & Baines (1963)	0·375	—	Hot-wire measurements
Patrick (1967)	0·380	$\alpha = 0{\cdot}85, \beta = 0{\cdot}80$	Pressure measurements $\overline{W}_{m0}/\overline{U}_e \geqslant 6{\cdot}6$
Gordier (1959)	0·370	$\alpha = 0{\cdot}74, \beta = 0$	Total pressure measurements in water
Present experiment	0·385	$\alpha = 1, \beta = 1{\cdot}53$	Hot-wire measurements $2{\cdot}37 \leqslant \overline{W}_{m0}/\overline{U}_e \leqslant 6{\cdot}36$

TABLE 1

Equations (1) and (2) for values of a between 2·37 and 6·35 agree well with the results obtained by various workers as shown in table 1.

This first study enabled the validity of an experimental procedure very often used in the determination of the jet axis to be verified. This procedure consists of defining the axis of the wreath geometrically from flow-pattern photographs (cf. Margason 1968). By this process, although there are obvious reservations concerning its degree of precision, it is nevertheless possible to obtain results close to those obtained by defining the axis as outlined above, as shown in figure 5 (plate 1).

2.4. *Evolution of the axial velocity*

Designating the value of the velocity along the jet axis by $\overline{W}_{\max}$, figure 6 indicates the law of variation

$$[\overline{W}_{\max}/(\overline{W}_{\max})_0]^{-1} = f(\zeta/r_0), \tag{3}$$

where ζ represents the curvilinear co-ordinate along the jet axis. It should be remembered that, in the case of a turbulent cylindrical jet flowing into a calm atmosphere, the law of decay of the axial velocity is hyperbolic in the steady state, so that (3) then becomes linear.

In the case of the jet flowing into a moving atmosphere such a law does not appear to be impossible, at least in certain zones of the flow.

2.5. *Velocity mapping*

From the raw results mentioned in § 2.2, the loci of the points where the magnitude of the velocity vector is constant, in the plane of symmetry of the flow, can be plotted. Thus three 'maps' corresponding to the three values of a (2.37, 3.95 and 6.35) are determined: figures 7 (*a*), (*b*) and (*c*).

These graphs reveal an interesting characteristic of the flow, namely its asymmetry, its axis being curved towards the lower boundary of the wreath. It is thought that this is due to the presence of a pressure field associated with the 'obstacle' formed by the wreath near its source and characterized by a zone of low pressure on the upstream face of the wreath.

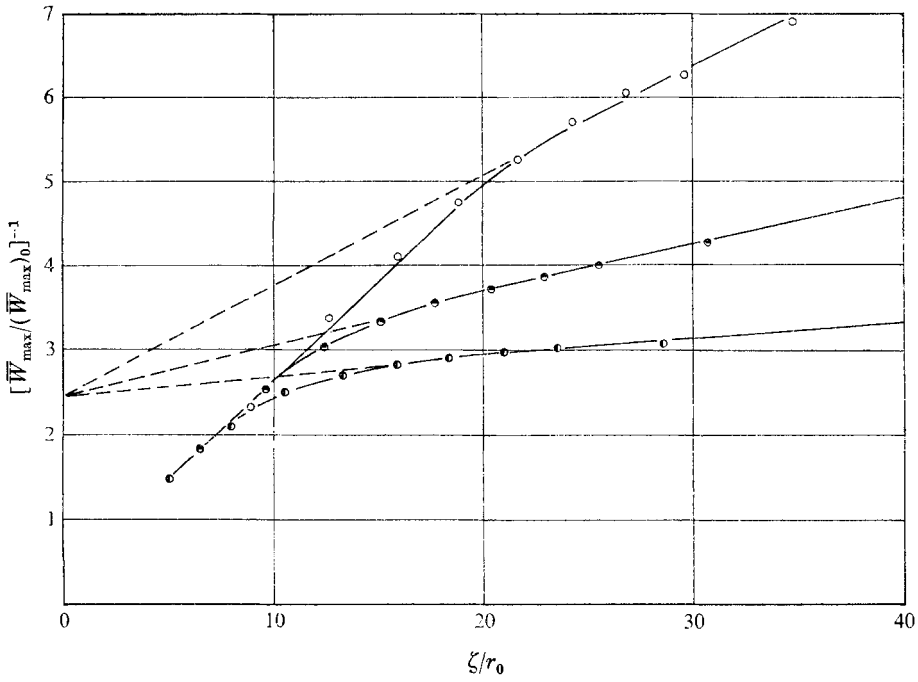

FIGURE 6. Axial velocity decay law. ○, $a = 6{\cdot}35$; ◓, $a = 3{\cdot}95$; ◐, $a = 2{\cdot}37$.

2.6. *Axial velocity profiles*

At various sections of the wreath, defined by their abscissae x_i/r_0, the profile of the velocity component parallel to the local tangent to the jet axis at x_i (corresponding to the angle on figure 8) was determined. Thus axial velocity $\overline{W}(r)$ profiles were obtained which were analogous to that represented in figure 9, which corresponds to the case $a = 3{\cdot}95$.

A method for extracting a law of similarity for these profiles to enable their representation by a single function was sought. This function was of the form

$$\overline{W}/\overline{W}_{max} = g(\eta), \tag{4}$$

where

$$\eta = r/r_\lambda, \tag{5}$$

r_λ being a reference length which should be specified.

A very conventional method of defining r_λ consists of choosing for it the distance from the axis to the point where the velocity is equal to $\lambda\overline{W}_{max}$. Because of the asymmetry of the velocity profile, such a process gives two different values of r_λ: r_λ^+ for $r > 0$ and r_λ^- for $r < 0$ (see figure 8). The non-dimensional variable η is then defined as follows:

$$\eta = \begin{cases} \eta^+ = r/r_\lambda^+ & \text{for} \quad r > 0, \\ \eta^- = r/r_\lambda^- & \text{for} \quad r < 0. \end{cases}$$

From this definition, the representation defined in (4) and (5) is applicable after a certain distance from the source. Moreover, as shown by figure 10, it

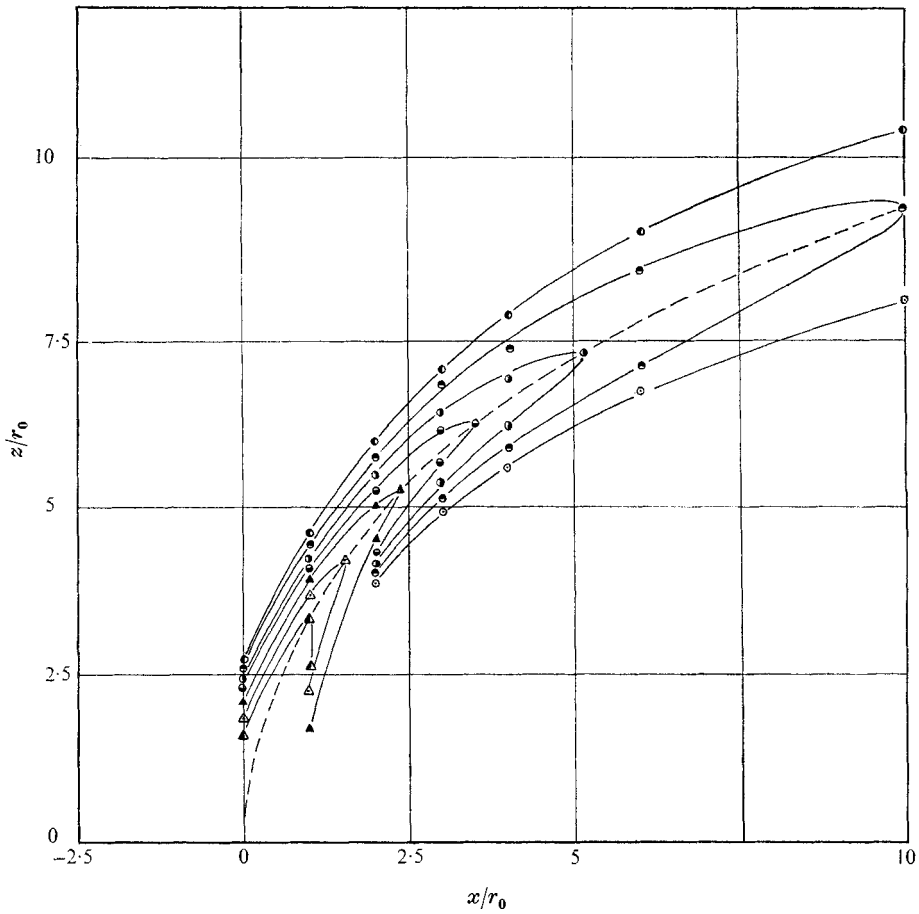

FIGURE 7 (*a*). For legend see p. 50.

leads to a symmetric curve of Gaussian type or a Tollmien function for the jet without cross-flow. The value of λ used for plotting figure 10 was the conventional value $\lambda = 0{\cdot}5$. The following can thus be concluded at this point.

(*a*) After a certain distance from the exit plane of the cylindrical jet deflected by a cross-flow, the non-dimensional axial velocity profiles $\overline{W}/\overline{W}_{\max}$ in the plane of symmetry of the flow depend only on the ratio $r/r_{\frac{1}{2}}$.

(*b*) As long as the points of the profile facing the cross-flow are related to $r_{\frac{1}{2}}^{+}$, and those downstream of the wreath to $r_{\frac{1}{2}}^{-}$, the non-dimensional profile obtained is symmetrical.

(*c*) The relationship $\overline{W}/\overline{W}_{\max} = g(\eta)$ thus obtained is closely analogous to that relating to a jet flowing into a calm atmosphere and can thus be represented, for example, by Tollmien's law.

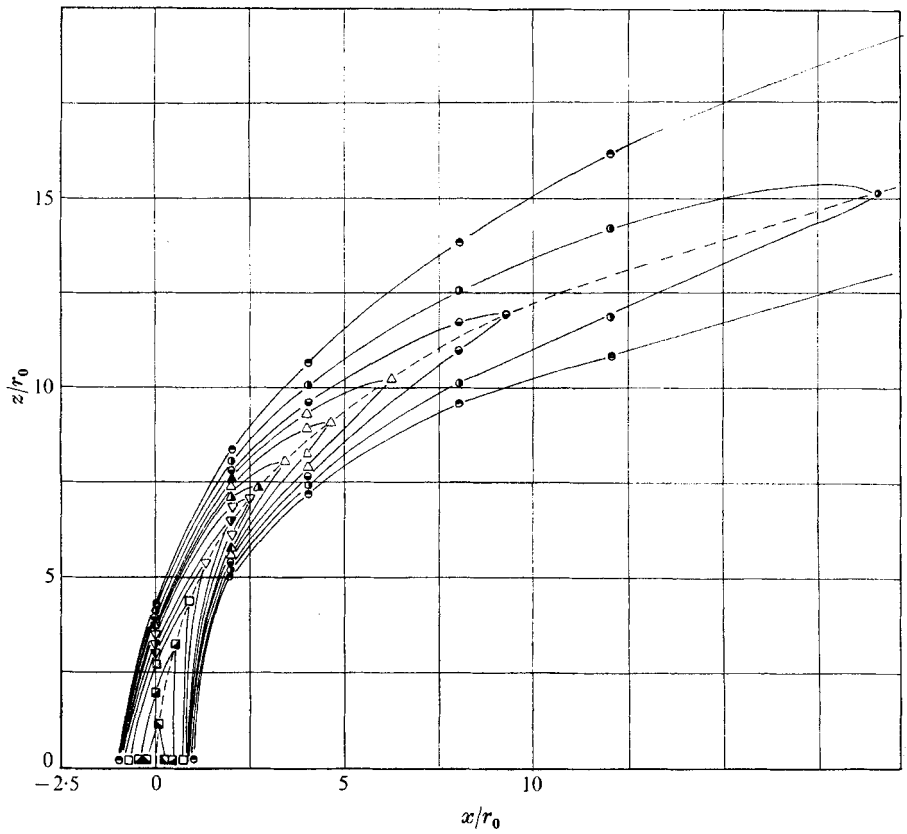

FIGURE 7 (*b*). For legend see p. 50.

2.7. *Law of variation of the wreath thickness*

Calling the thickness of the wreath $B_{\lambda 0}(x)$ to $O(1-\lambda_0)$ accuracy, we have

$$B_{\lambda 0}(x) = |r^+_{\lambda_0}(x)| + |r^-_{\lambda_0}(x)|. \tag{6}$$

Figure 11 then shows the variation of $r^+_{\lambda_0}(x)$ and $r^-_{\lambda_0}(x)$ to be linear and of differential gradient as could be expected (the value chosen for λ_0 was 0·50).

From (6) it can be deduced that the thickness of the wreath varies linearly with longitudinal distance downstream of the jet, a result which should be compared with the widely accepted hypothesis that the 'width' of the wreath follows a relationship linear in x.

2.8. *Some remarks on the flow at the periphery of the jet*

The first remark concerns the presence of a 'secondary flow' in the wake zone. The velocity measurements showed, moreover, that this occurs either in the same direction as the jet or in the opposite direction, thus leading to a real reverse current. This phenomenon may be likened to that of the 'crest' noted in many experiments on hydraulic models; see Vadot (1965). In the upper part of the jet,

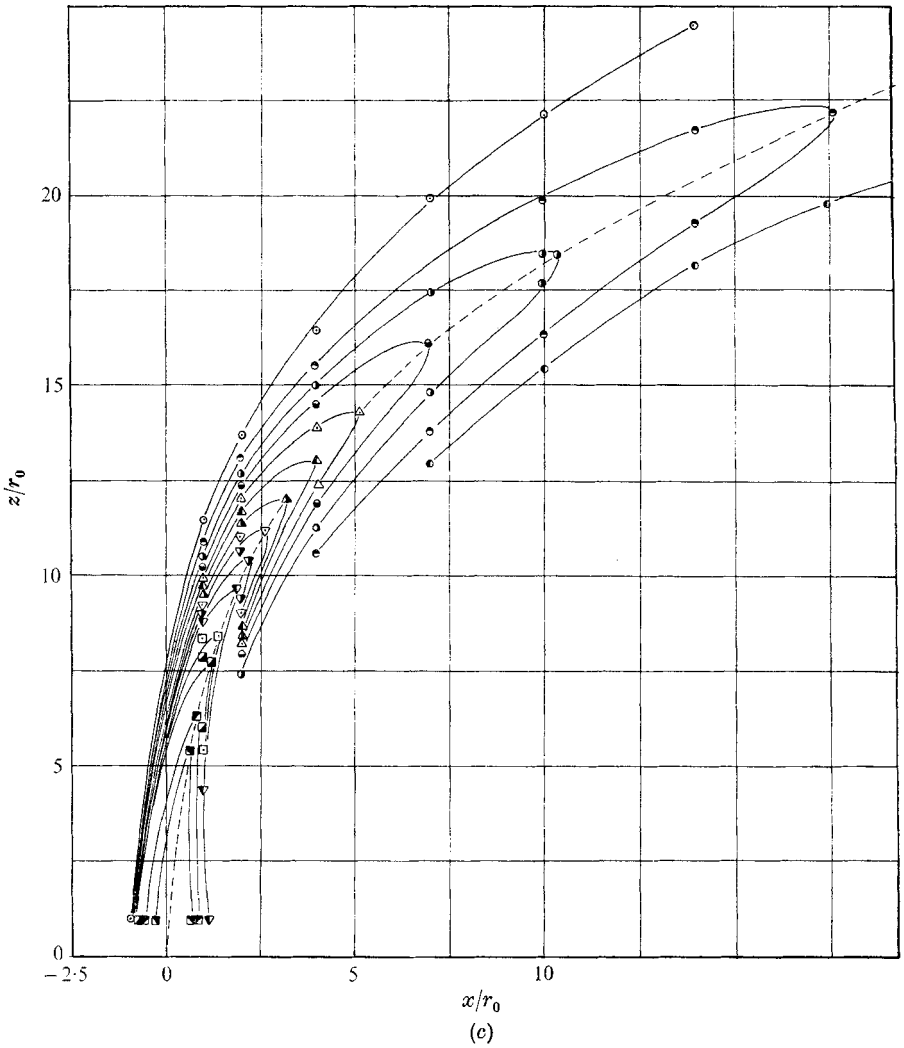

FIGURE 7. Velocity maps of the sheared single jet. (*a*) $\overline{W}_{m0} = 8{\cdot}17$ m/s, $a = 2{\cdot}37$, $Re_0 = 21200$. (*b*) $\overline{W}_{m0} = 16{\cdot}95$ m/s, $a = 3{\cdot}95$, $Re_0 = 41500$. (*c*) $\overline{W}_{m0} = 20{\cdot}70$ m/s, $a = 6{\cdot}35$, $Re_0 = 53600$. ––, jet axis.

Velocity (m/s)	3	3·5	4	5	6	7	8	9	10	11	12	14	16	18
			(*b*)					(*c*)						
Velocity (m/s)				19					19	20	21			

on the other hand, such a phenomenon is not present, which helps to show the previously mentioned asymmetry.

The second remark deals with the formation of a stable eddy system downstream of the jet. At several different points M of a particular vertical section, the Euler autocorrelation $\overline{u'_M(t)\,u'_M(t-\tau)}$ was recorded. The curves obtained, which appear for qualitative reasons only in figure 12, show clearly the appearance of a periodic phenomenon of much lower frequency than the turbulent fluctuations, and thus indicate the existence of a stable eddy system in this zone of the flow.

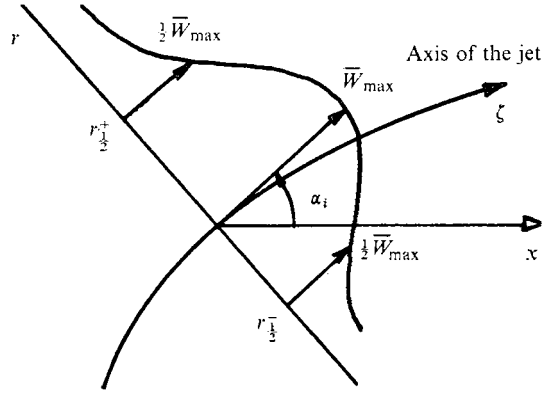

FIGURE 8

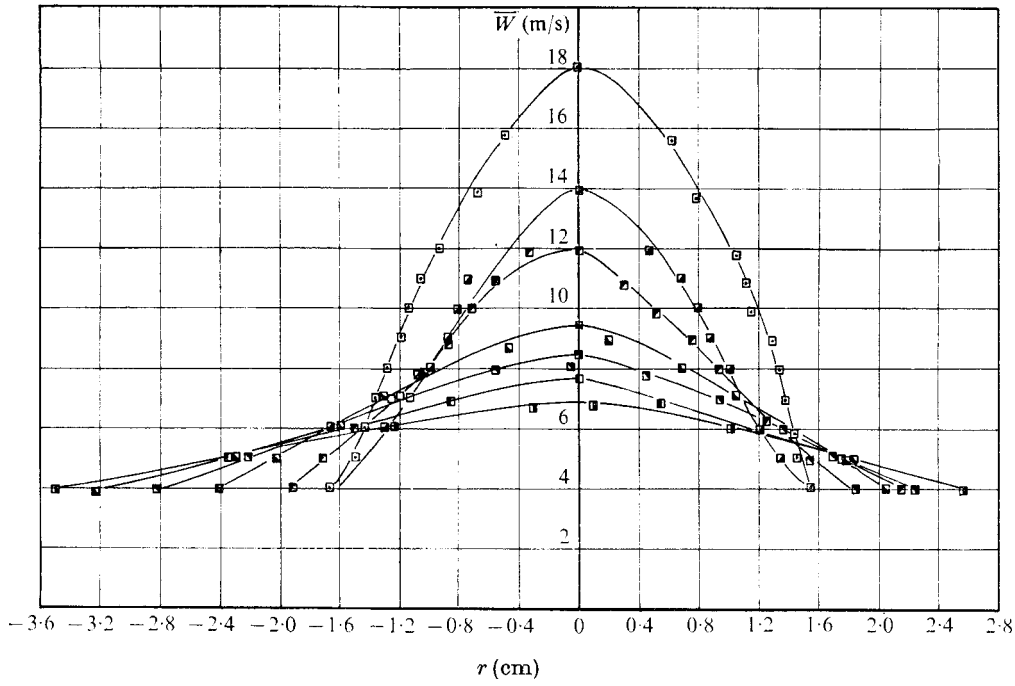

FIGURE 9. Axial velocity profiles in the deflected jet. $a = \overline{W}_{m0}/\overline{U}_e = 3{\cdot}95$

x/r_0	0·5	1·25	2·0	3·0	4·0	5·0	6·0

2.9. *New method for calculating the jet axis in the zone of velocity profile similarity*

The experimental results already mentioned can be used as a starting-point for a new method for evaluating the axis of the jet under the influence of a transverse shear. Consider, in the zone of establishment of velocity profile similarity, the

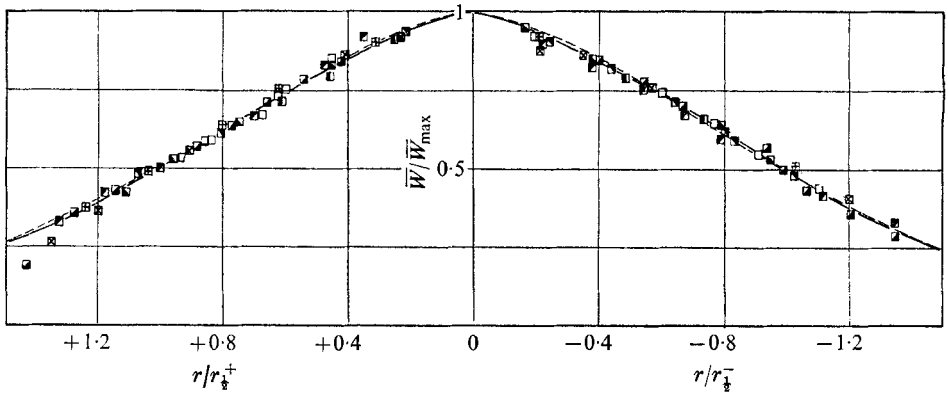

FIGURE 10. Similarity law for axial velocity profiles in the deflected jet. For $a = 6{\cdot}35$: ⊠, $x/r_0 = 2$, ⊞, $x/r_0 = 4$; – –, theoretical Tollmien law. For $a = 3{\cdot}95$: ◪, $x/r_0 = 1{\cdot}25$; ◩, $x/r_0 = 2$; □, $x/r_0 = 3$; ◥, $x/r_0 = 4$; ◨, $x/r_0 = 5$.

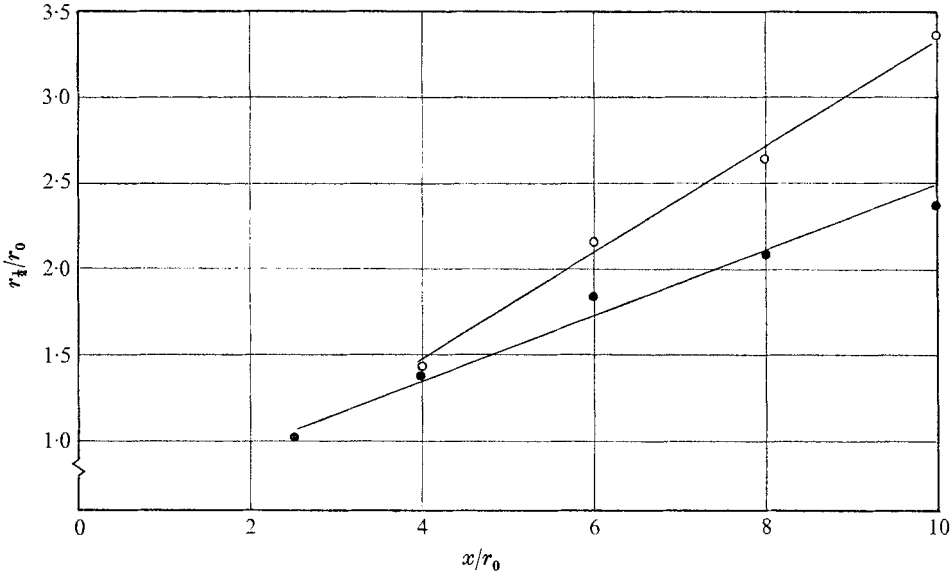

FIGURE 11. Variation of jet thickness with longitudinal distance. $\overline{W}_{m0} = 16{\cdot}95$ m/s, $a = 3{\cdot}95$, $Re_0 = 41\,500$. ○, $r_{\frac{1}{2}}^{+}$; ●, $r_{\frac{1}{2}}^{-}$.

half-profile of the axis component connected with the upper part of the jet. The boundary conditions are

$$\overline{W} = \begin{cases} \overline{W}_{\max} & \text{at} \quad r = 0, \\ \lambda \overline{U}_e \cos\alpha & \text{at} \quad r = r_\lambda. \end{cases}$$

Allowing for the effect of the non-dimensional variable $\eta = r/r_\lambda$ and taking into account equation (4), the following is true at the upper boundary:

$$\overline{W}(1, \zeta/r_0) = \lambda \overline{U}_e \cos\alpha = g(1)\overline{W}_{\max};$$

substituting (3) in this equation yields the following:

$$\lambda \overline{U}_e \cos\alpha = \frac{g(1)}{f(\zeta/r_0)} (\overline{W}_{\max})_0.$$

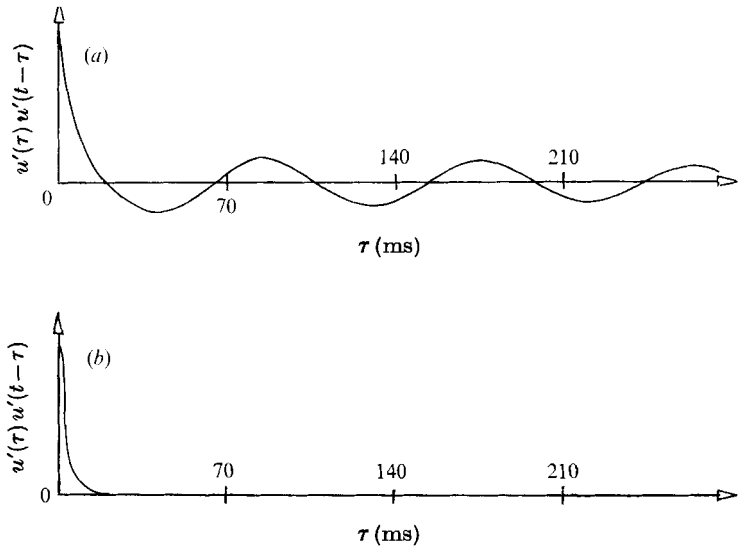

FIGURE 12. (*a*) Periodic phenomenon and (*b*) its disappearance at $x/r_0 = 5$. $\overline{W}_{m0} = 20{\cdot}70$ m/s, $a = 6{\cdot}35$, $Re_0 = 53\,600$. (*a*) $z/r_0 = 8$, frequency $\simeq 11{\cdot}5$ Hz. (*b*) $z/r_0 = 10$.

Then, if the fact that $\cos\alpha = dx/d\zeta$ is used in this equation, the differential equation of the wreath axis in the form $x(\zeta)$ is obtained:

$$dx = \frac{(\overline{W}_{\max})_0}{\overline{U}_e}\frac{g(1)}{\lambda}\frac{d\zeta}{f(\zeta/r_0)}.$$

If the suffix 1 is assigned to the section from which the similarity is established, integration yields

$$x - x_1 = \frac{(\overline{W}_{\max})_0}{\overline{U}_e}\frac{g(1)}{\lambda}\int_{\zeta_1}^{\zeta}\frac{dt}{f(t/r_0)}. \tag{7}$$

Equation (7) shows that continuation of the evaluation now depends only on a knowledge of the axial velocity decay law, characterized by the function $f(\zeta/r_0)$. As a first approximation, as suggested by figure 3, a linear relationship is assumed. Then letting

$$A = \frac{(\overline{W}_{\max})_0}{\overline{U}_e}\frac{g(1)}{\lambda} \tag{8}$$

and

$$f(\zeta/r_0) = K\zeta/r_0 + K', \tag{9}$$

equation (7) leads to

$$\frac{x}{r_0} - \frac{x_1}{r_0} = \frac{A}{K}\log\left(\frac{K\zeta/r_0 + K'}{K\zeta_1/r_0 + K'}\right), \tag{10}$$

which constitutes the jet axis in (x, ζ) co-ordinates.

In order to obtain the equation in (z, x) co-ordinates, it is sufficient to note that

$$dz/d\zeta = (1 - \cos^2\alpha)^{\frac{1}{2}}, \quad \text{where} \quad \cos\alpha = dx/d\zeta.$$

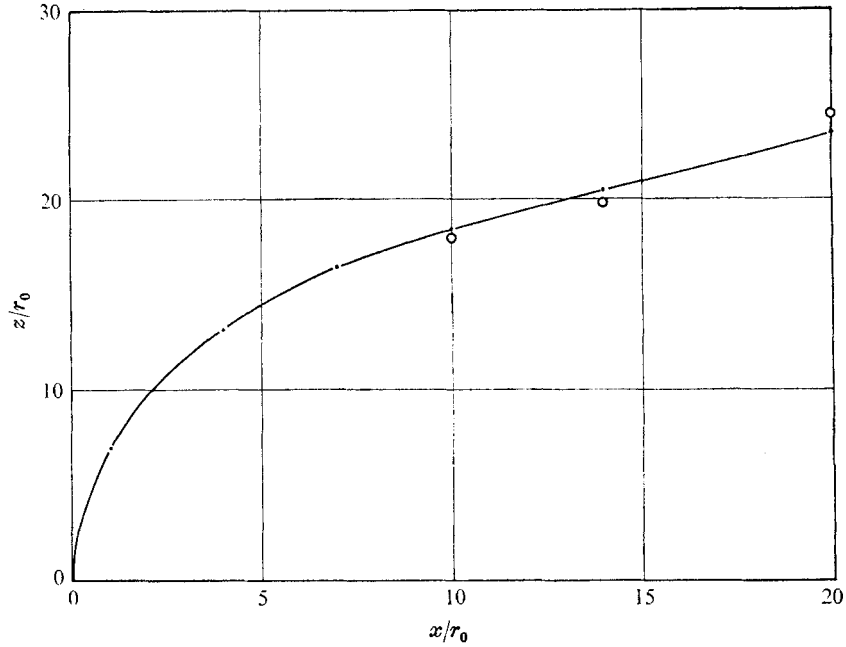

FIGURE 13. Comparison of theoretical (curve) and experimental (points) jet axes; $a = 6{\cdot}25$.

x/r_0	1	4	7	10	14	20
z/r_0						
Experimental	7	13·2	16·5	18·2	20·5	23·5
Theoretical	—	—	—	17·94	19·86	24·47
$\frac{(z/r_0)_{\text{exp}} - (z/r_0)_{\text{th}}}{(z/r_0)_{\text{th}}}$ (%)	—	—	—	+1·7	+3·2	−4

Thus, putting
$$u = K\zeta/r_0 + K' \tag{11}$$
gives
$$d\left(\frac{z}{r_0}\right) = \frac{1}{K}(u^2 - A^2)^{\frac{1}{2}}\frac{du}{u}, \tag{12}$$
integration of which gives
$$K\left(\frac{z}{r_0} - \frac{z_1}{r_0}\right) = \int_{u_1}^{u} \frac{(t^2 - A^2)^{\frac{1}{2}}}{t}\,dt. \tag{13}$$

By putting $t = A\cosh\phi$, the indefinite form of the integral on the right-hand side can also be written as $A\int \tanh\phi \sinh\phi\, d\phi$, which can be integrated by parts to give the expression $A[\sinh\phi - 2\tan^{-1}(\tanh\frac{1}{2}\phi)]$.

Returning to the variables z/r_0 and $X = x/r_0 = x_1/r_0$, the equation of the jet axis can be written in the form
$$\frac{z - z_1}{r_0} = \frac{1}{K}\left\{[u_1^2\exp(2KA^{-1}X) - A^2]^{\frac{1}{2}} - 2\tan^{-1}\left(\frac{u_1\exp(KA^{-1}X) - A}{(u_1^2\exp(2KA^{-1}X) - A^2)^{\frac{1}{2}}}\right)\right.$$
$$\left. - (u_1^2 - A^2)^{\frac{1}{2}} + 2\tan^{-1}[u_1 - A/(u_1^2 - A^2)^{\frac{1}{2}}]\right\}, \tag{14}$$
where u_1 is simply $K(\zeta_1/r_0) + K' = f(\zeta_1/r_0)$.

An illustration of the above calculation is given by figure 13 for the case where $\overline{W}_m/\overline{U}_e = 6{\cdot}35$. Profile similarity was assumed to hold from the section $x_1/r_0 = 10$, where $\zeta_1/r_0 = 20{\cdot}9$. The decay of the axial velocity was taken as a hyperbolic

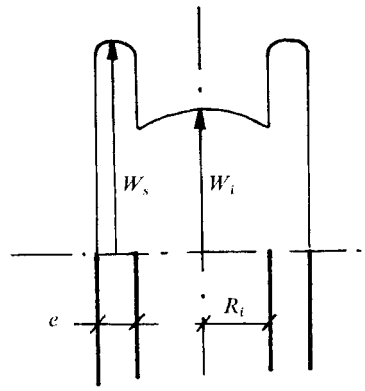

FIGURE 14

function, leading to a linear expression for the function $f(\zeta/r_0)$ where $K = 0{\cdot}13$ and $K' = 0{\cdot}25$, these values being deduced from the appropriate curve of figure 6. The numerical values of the other parameters were $A = 5{\cdot}05$ and $u_1 = 5{\cdot}20$. In the caption to figure 13, the divergence between the theoretical and experimental points is given. It is less than or equal to 4 % within the range

$$10 \leqslant x/r_0 \leqslant 20.$$

It should be noted, however, that the approximation of the function $f(\zeta/r_0)$ by a linear relationship leads to an axis equation which diverges very rapidly as x/r_0 tends towards infinity. Also such a simplification, from the calculation viewpoint, is not necessarily the most appropriate, and a more elaborate form (such as a power law) might lead to results whose range of validity was greater.

3. Study of coaxial jets

3.1. *Introduction*

In parallel with the study of a jet sheared by a cross-flow, the shear of two coaxial jets by a similar cross-flow was also studied. These coaxial jets were generated by two concentric cylindrical ducts with independent supplies.

The tests described were characterized by the following non-dimensional experimental conditions: e/R_i, $\overline{W}_s/\overline{W}_i$ and $\overline{W}_i/\overline{U}_e$, where R_i and $R_i + e$ are the respective radii of the internal and external ducts, $\overline{W}_i$ and $\overline{W}_s$ are the respective exit velocities of the internal and external jets and $\overline{U}_e$ is the velocity of the cross-flow (see figure 14). As before, the mean velocity direction was determined by pressure sensors, and its magnitude by hot-wire anemometry.

3.2. *Characteristics of the tests*

The experimental results discussed satisfy the characteristics given in table 2, among which ambient pressure P_a and temperature T_a are also quoted.

3.3. *Definition of the jet axis*

Having defined the jet axis as the locus of the velocity maxima in the case of a single jet, a slightly analogous definition was adopted for axis of the coaxial

Parameter	R_i (mm)	e/R_i	$\overline{W}_i$ (m/s)	$\overline{W}_o/\overline{W}_i$	$\overline{U}_e$ (m/s)	$\overline{W}_i/\overline{U}_e$	P_a (mm Hg)	T_a (°C)
Test *A*	20	0·05	10·7	8	3	3·56	750	22
Test *B*	20	0·10	10·7	4	3	3·56	748	21
Test *C*	20	0·05	10·7	5·5	3	3·56	755	23

TABLE 2

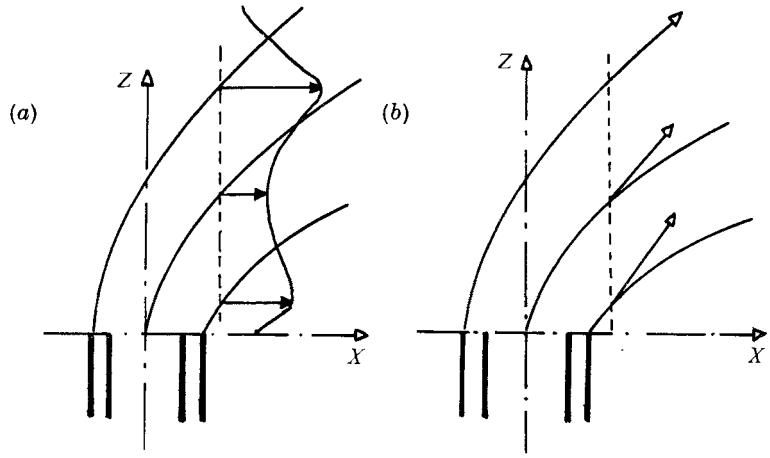

FIGURE 15. Vertical velocity profiles. (*a*) Magnitude. (*b*) Direction.

jets, following a study of the vertical profiles of the magnitude and direction of the velocity (figures 15 (*a*) and (*b*)). Near the nozzles, each profile of the velocity magnitude has two maxima: one facing the cross-flow, the other downstream of the jet. After the respective maxima facing the cross-flow and downstream of the jet had been plotted, it was noted (figure 15) that only the locus of the maxima facing the cross-flow is a line of mean velocity, the locus of the maxima downstream of the jet being inclined at an angle to the direction of the mean velocity at every point. The behaviour of the velocity downstream of the jet can be explained by considering that two regions of eddies develop on either side of the plane of symmetry of the flow with ingestion of external air into the jet (see figure 16).

In consequence the jet axis was defined as the locus of the maxima facing the cross-flow.

3.4. *Isovels: evolution of the velocity maxima facing the cross-flow*

From the velocity measurements taken, it was possible to plot lines of constant velocity magnitude for the three cases considered (figure 17). In order to do this, a few particular values of the magnitude of the mean velocity were plotted, these being obtained by exploring the vertical velocity profiles.

From the preceding results, the position of the jet axis, i.e. the locus of the velocity maxima facing the cross-flow, was studied (figure 18).

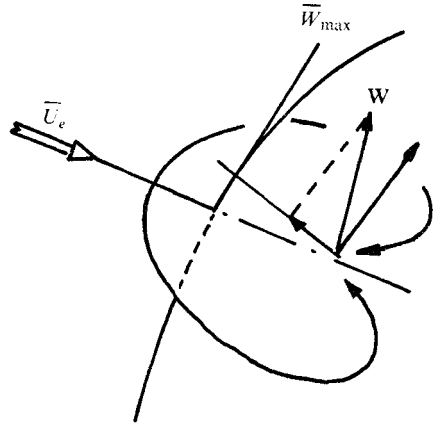

FIGURE 16

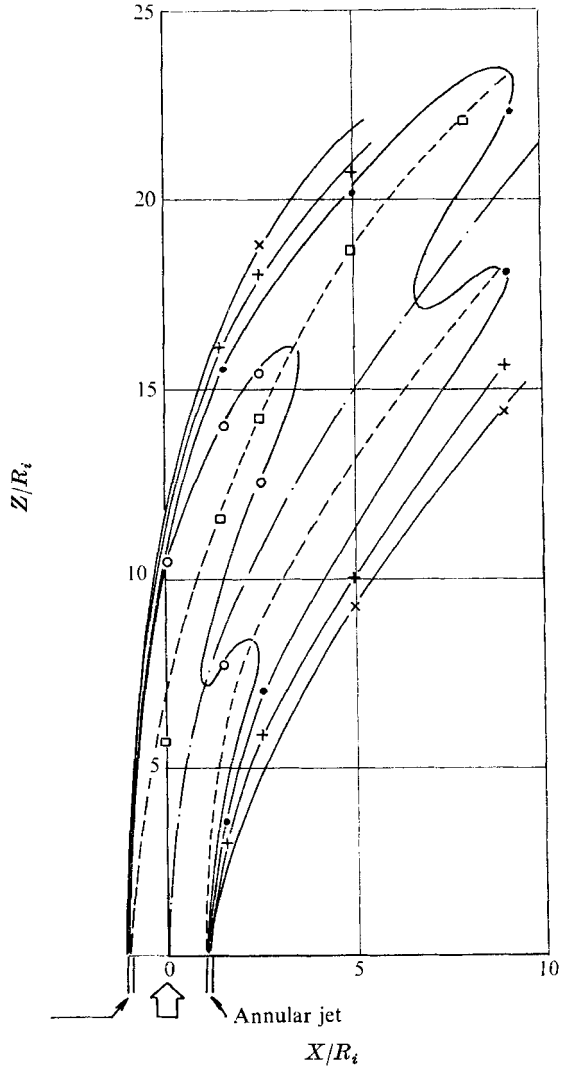

FIGURE 17 (*a*). For legend see p. 59.

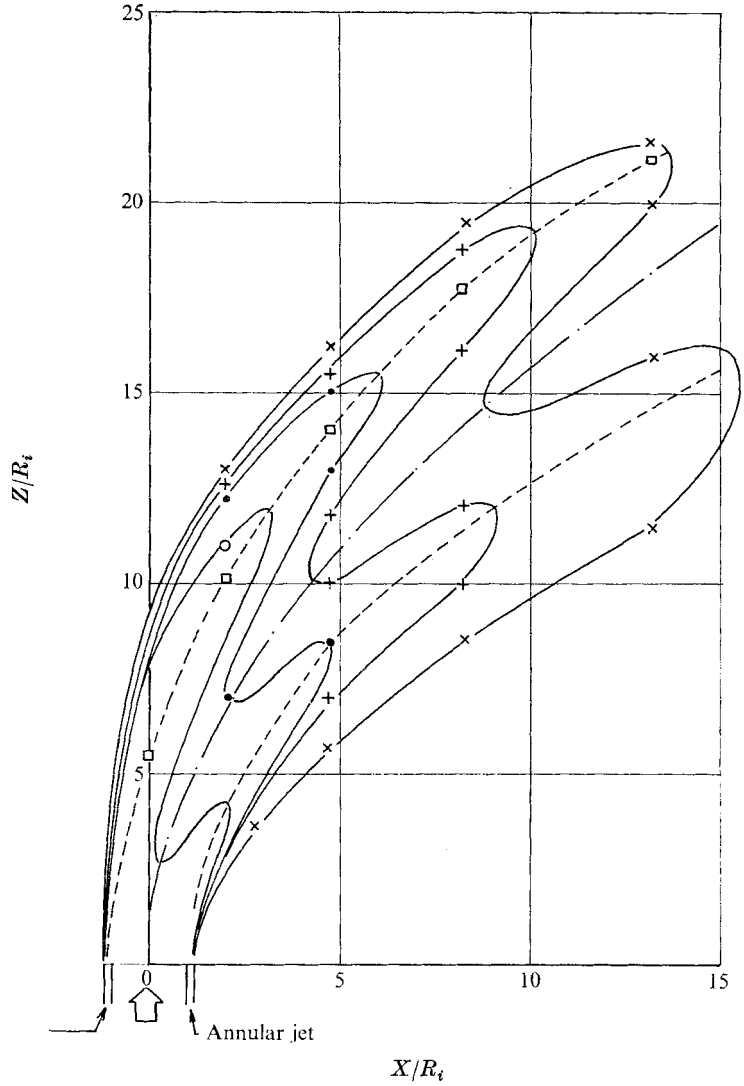

FIGURE 17 (*b*). For legend see p. 59.

3.5. *Evolution of the jet axis*

The determination of the axis of the jets was achieved with the help of the isovels, of which the most advanced points form part of the axes. It was shown that the axis of the jets may be expressed by a power law for the fully developed flow.

Indeed the variation of $\log (Z/R_i)$ with $\log (X/R_i)$, where Z/R_i and X/R_i are non-dimensional, is linear with slope $\alpha = 0{\cdot}385$ (figure 19). Thus

$$Z/R_i = K(X/R_i)^{0{\cdot}385}, \tag{15}$$

where $K = 9{\cdot}45$, $7{\cdot}50$ and $7{\cdot}00$ for tests A, B and C respectively (experimental values). This result, which is identical to that for the single jet, differs nevertheless in the determination of the coefficient K.

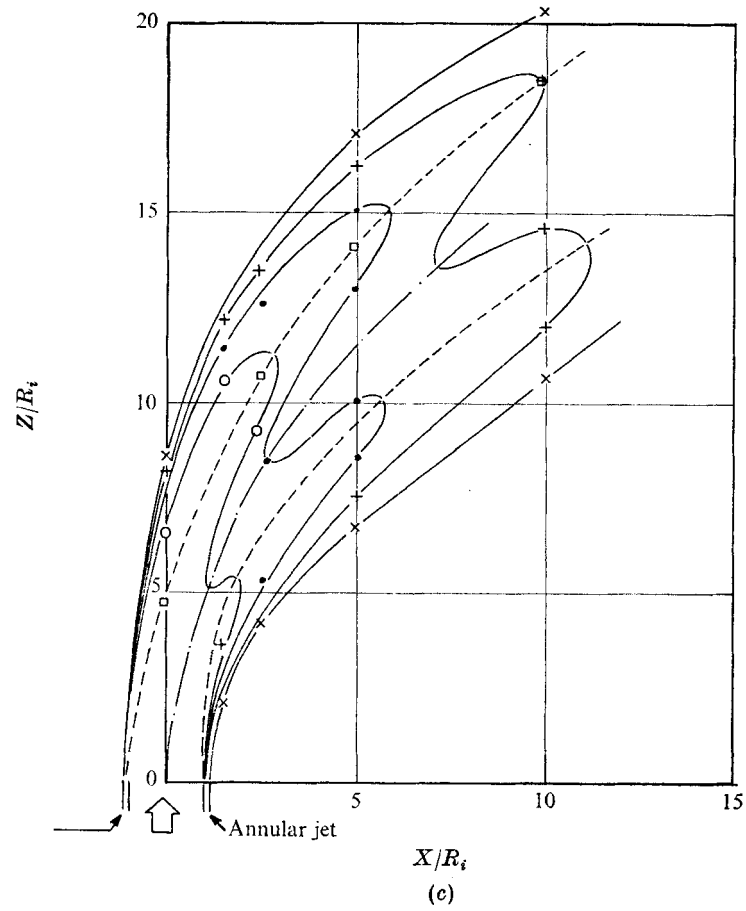

FIGURE 17. Velocity maps for the coaxial jets. □, maximum velocity; ×, 4 m/s; +, 5 m/s; ●, 6 m/s; ○, 10 m/s. (*a*) Test *A*, annulus thickness = 1 mm. (*b*) Test *B*, annulus thickness = 2 mm. (*c*) Test *C*, annulus thickness = 1 mm.

The following formula, a function of the characteristic test parameters e, R_i, $\overline{W}_i$, $\overline{W}_s$ and $\overline{U}_e$ and of the mean velocity $\overline{W}_{is}$, is suggested for K:

$$K = 1{\cdot}53 + 0{\cdot}6\,(\overline{W}_{is}/\overline{U}_e) + 0{\cdot}2\,(e/R_i)\,(\overline{W}_s/\overline{W}_i)^2\,(\overline{W}_i/\overline{U}_e)^{\frac{3}{2}}, \tag{16}$$

where

$$\overline{W}_{is} = \frac{\text{central flow} + \text{annular flow}}{\text{cross-section of the central duct}}.$$

This relation for K was obtained by taking measurements from photographs of jets taken during tests during which each characteristic parameter was systematically and independently varied.

Finally, good agreement between the experimental and calculated values for K was obtained with calculated values for K of 9·68, 7·53 and 7·00 for tests A, B and C respectively.

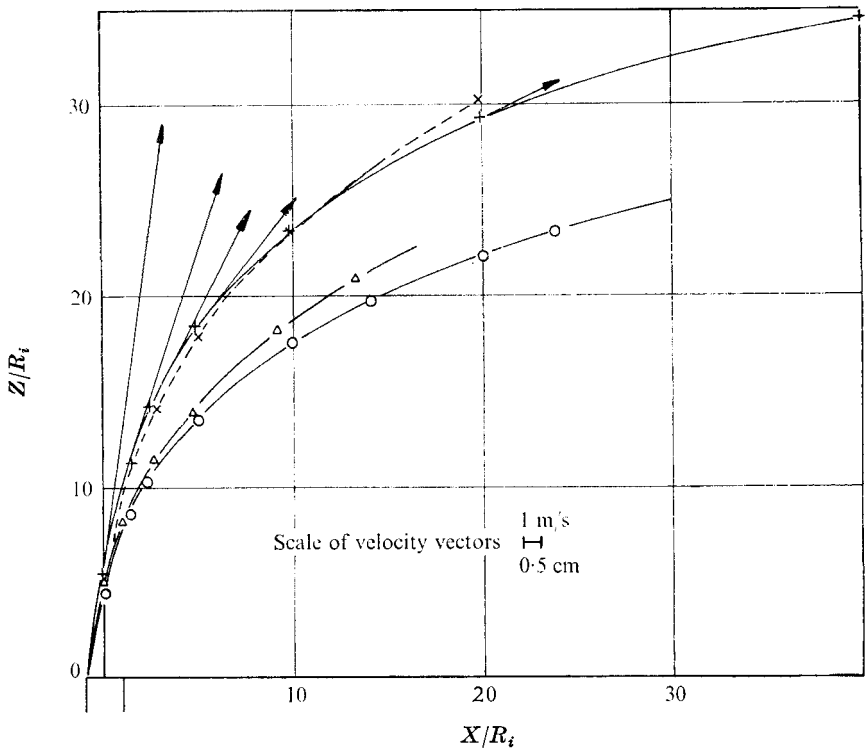

FIGURE 18. Jet axis. $U_e = 3$ m/s: +, test A; △, test B; ○ test C. – – × – –, axis calculated from (15) and (16).

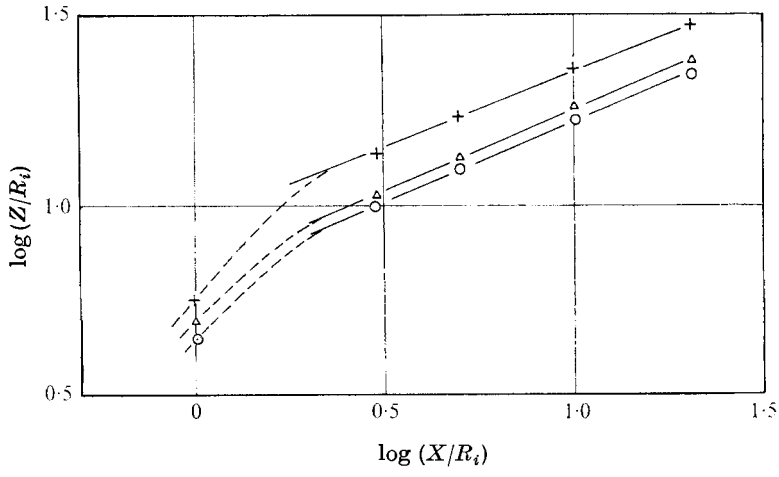

FIGURE 19. Law of variation of the jet axis. Slope α of the linear part is 0·385. +, test A; △, test B; ○, test C.

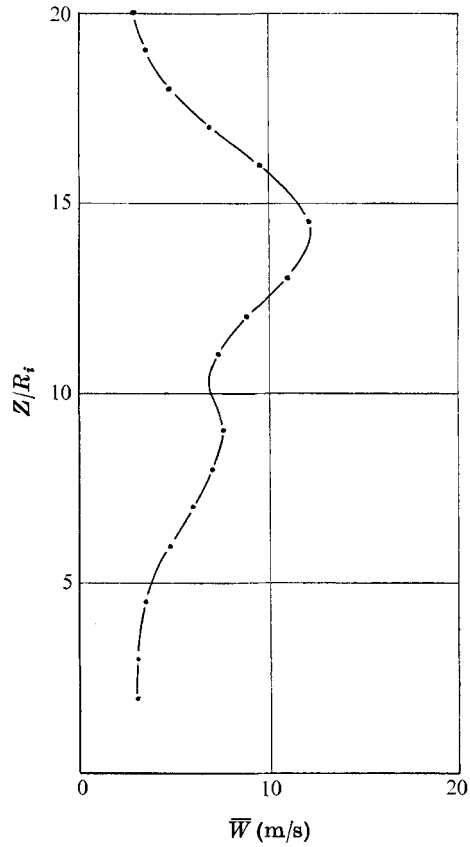

FIGURE 20. Example of velocity magnitude profile: test *A*.

3.6. *Transverse velocity profiles*

By using the magnitudes from the isovels and by projecting these, taking into account the mean direction of the velocity at each point, onto the normal to the jet axis, several transverse mean velocity profiles were plotted. One of these is supplied as an example in figure 20. The strong asymmetry of these profiles stresses the decisive role played by the velocity maximum facing the cross-flow.

3.7. *High-speed central jet*

If the velocity relationship of the central and annular jets is reversed and shear takes place through a cross-flow perpendicular to the jet axis, separation of the two jets occurs. The central high-speed jet pierces the annular jet, thus losing part of its energy and continuing its trajectory as a single jet, whilst the annular jet, having been entrained for a short while by the central jet, in turn behaves as a single sheared jet. The readings of the velocity maxima plotted on figure 21 show the two distinct paths for the jets.

In this particular case, dissociation of the two flows is confirmed. This

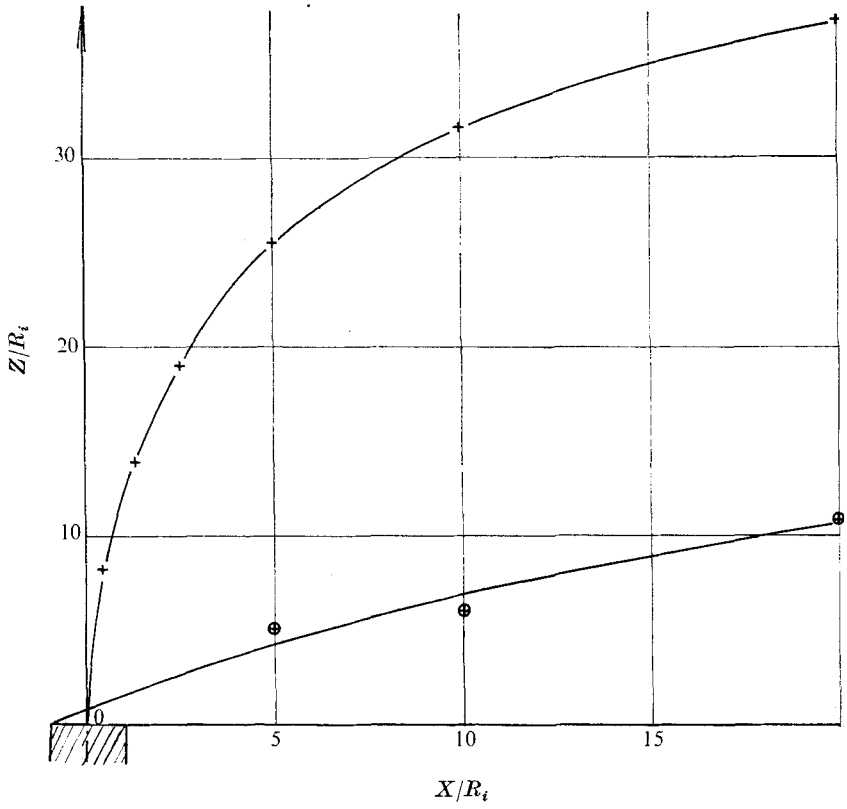

FIGURE 21. Central blowing: locus of velocity maxima. $\overline{W}_s/\overline{W}_i = 0{\cdot}11$. +, central jet; ⊕, annular jet.

phenomenon does not occur in the absence of a cross-flow, mixture then taking place through entrainment of the external jet by the central jet; see Mermet, Bouscaren & Dubois (1966).

3.8. *High-speed blowing with a semicircular annulus round the central jet*

The results of the study described in §3 showed that the high-speed annular jet delays the effects of the shearing of the central jet by a cross-flow. Because of the asymmetry of the velocity profile already mentioned it seems that the annular jet does not contribute in its entirety in the same manner to this phenomenon. Thus it was interesting to study the behaviour of the central jet for the case when the annular blowing was limited to the upstream semicircle.

After defining the jet axis as in §3 the relation $Z/R_i = f(X/R_i)$ was plotted in figure 22 for the experimental conditions given in table 3.

It was noted that, contrary to the previous case where $W_s/W_i < 1$, entrainment takes place without separation of the two jets as in the case where blowing occurs round the entire annulus. However, it should be pointed out that the height of penetration is now smaller.

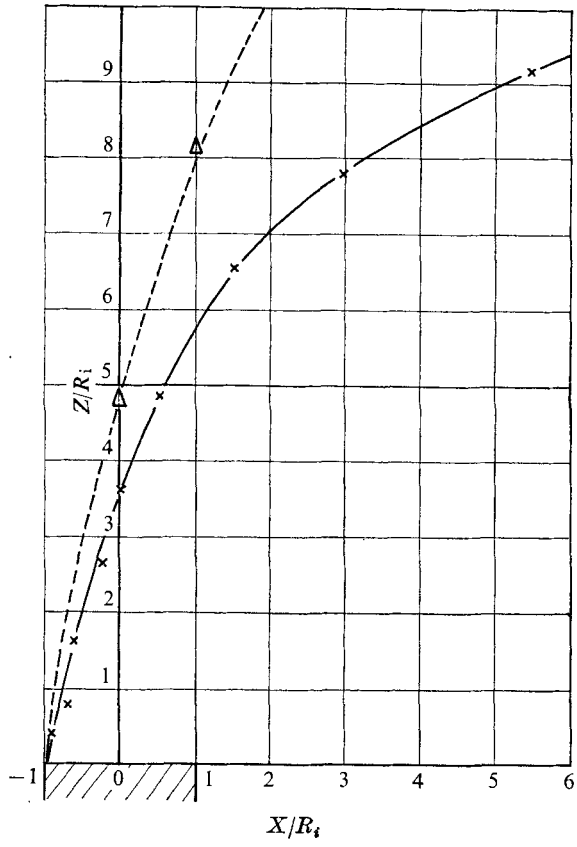

FIGURE 22. $Z/R_i = f(X/R_i)$ *vs.* X/R_i. ——, semicircular upstream blowing; – –, annular blowing, test *B*. $\overline{W}_s/\overline{W}_i = 4$, $\overline{U}_e = 3$ m/s.

R_i (mm)	e/R_i	$\overline{W}_i$ (m/s)	$\overline{W}_s/\overline{W}_i$	$\overline{U}_e$ (m/s)	P_a (mm Hg)	T_a (°C)
20	0·10	10·7	4	3	751	21

TABLE 3

4. Conclusions

The preceding sections have enabled a certain number of results to be obtained concerning the behaviour of two types of turbulent jet being acted upon by a cross-flow. In the case of the initially cylindrical single jet, the velocity distribution measurements led to a stricter definition of the flow in the plane of symmetry. Thus it was possible to define not only the axes of the jets, but also the axial velocity component profiles and the evolution of the component maximum along the axis. The analysis thus carried out enabled a zone of velocity profile similarity to be found, in which the jet axis equation is closely linked to the expression for the decay of the maximum velocity. This connexion can then be used as a

basis for a new calculation method for the jet axis depending not on considerations of overall equilibrium of a finite element of the jet, but on the intrinsic structures of the flow. Conversely, starting with the equation of the jet axis, it thus becomes possible to deduce a relationship for the axial velocity decay.

For the second part of the study, concerning the emission of coaxial jets into a cross-flow, there exists as yet, as far as the authors know, only a very limited amount of literature. This is why the first aim was to define the overall characteristics of the flow embodying the jet axes and the velocity 'maps'. The fundamental parameter considered in these tests is the ratio $\overline{W}_s/\overline{W}_i$ of the initial exit velocities of the two jets, which has a very direct influence on the height of penetration. In particular, high-speed annular blowing can be considered as a method of delaying the effects of shearing of the central jet by the cross-flow. This result is close to the statements made by Madjirski, Tchitchov & Kouzou (1970) on the existence near the nozzles of a separation surface between the central and annular jets in a calm atmosphere and those of Ricou & Spalding (1961) concerning the importance of delaying the turbulent dilution of the central jet until a long distance from the nozzles. This leads to interest in the effect of this parameter on the diffusion conditions.

On this point, it is found that blowing with only the semicircle facing the cross-flow leads to results analogous to those obtained by blowing over the whole annulus for the case when $\overline{W}_s/\overline{W}_i > 1$. On the other hand inversion of the blowing jets ($\overline{W}_s/\overline{W}_i < 1$) leads to separation of the jets and drastically affects the diffusion conditions of the flow.

REFERENCES

Abramovitch, M. 1963 *The Theory of Turbulent Jets.* M.I.T. Press.

Akatnov, N, I. 1969 *Izv. Akad. Nauk. S.S.S.R. Mekh. Zh. Gaz.* **6**, 11–19.

Callaghan, E. E. & Ruggeri, R. S. 1948 *N.A.C.A. Tech. Note*, no. 1615.

Callaghan, E. E. & Ruggeri, R. S. 1951 *N.A.C.A. Tech. Note*, no. 2466.

Fan, L. N. 1967 *Keck Hyd. Lab. California Inst. Tech. Rep.* KH-R-15.

Gordier, R. L. 1959 *St Ant. Falls Hyd. Lab. Tech. Paper*, B 28.

Jordinson, R. 1956 *Aero. Res. Counc. R. & M.* no. 3074.

Keffer, J. F. & Baines, W. D. 1963 *J. Fluid Mech.* **15**, 481.

Madjirski, V., Tchitchov, E. & Kouzou, K. 1970 *Rev. Roum. Sci. Tech. Appl.* **15**, 1125–1138.

Margason, R. J. 1968 *N.A.S.A. Tech. Note*, D-4919.

Mermet, R., Bouscaren, R. & Dubois, E. 1966 *Sté Bertin. Note*, no. 25, p. 217.

Patrick, M. A. 1967 *J. Inst. Fuel*, **40**, 425–432.

Platten, J. L. & Keffer, J. F. 1968 *University of Toronto Mech. Engng Tech. Paper*, no. 6808.

Ricou, F. P. & Spalding, D. B. 1961 *J. Fluid Mech.* **11**, 21.

Ruggeri, R. S. 1952 *N.A.C.A. Tech. Note*, no. 2855.

Ruggeri, R. S., Callaghan, E. E. & Bowden, D. T. 1950 *N.A.C.A. Tech. Note*, no. 2019.

Shandorov, G. S. 1966 *Izv. Vyssh. Vchbn. Zaved. Akad. Tech. S.S.S.R.* **2**, 100–104.

Vadot, L. 1965 *Centre Interprofessionnel Technique d'Etudes de la Pollution Atmosphérique (Paris). Etude faite par SORGEAH*, Grenoble, France.

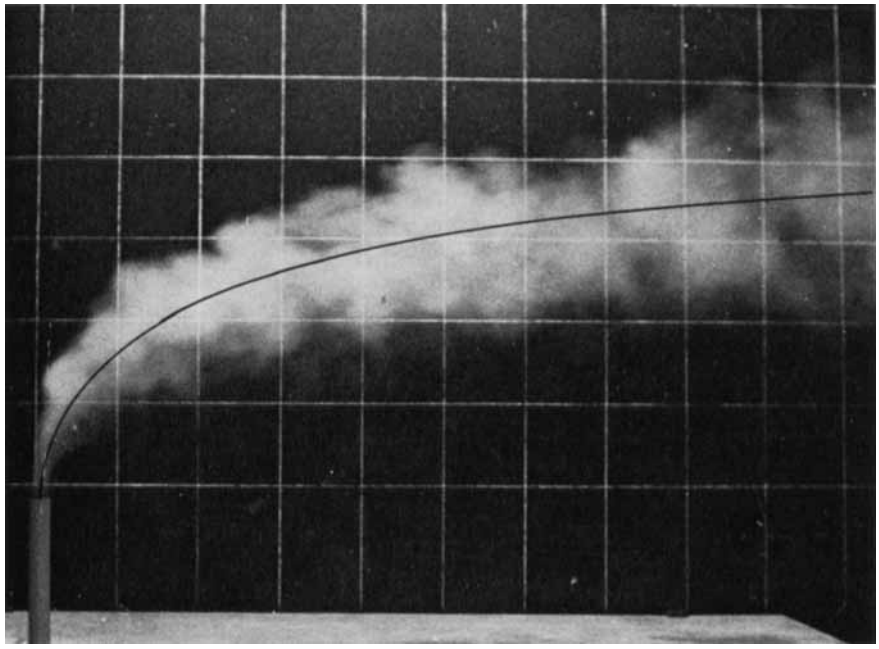

FIGURE 5. Flow pattern for the case $a = 6{\cdot}25$. ——, jet axis, defined as the locus of the velocity maxima.